Mitochondrial Cardiomyopathy Caused by Elevated Reactive Oxygen Species and Impaired Cardiomyocyte Proliferation

Donghui Zhang,* Yifei Li,* Danielle Heims-Waldron, Vassilios Bezzerides, Silvia Guatimosim, Yuxuan Guo, Fei Gu, Pingzhu Zhou, Zhiqiang Lin, Qing Ma, Jianming Liu, Da-Zhi Wang, William T. Pu

Rationale: **Although mitochondrial diseases often cause abnormal myocardial development, the mechanisms by which mitochondria influence heart growth and function are poorly understood.**

Objective: **To investigate these disease mechanisms, we studied a genetic model of mitochondrial dysfunction caused by inactivation of *Tfam* (transcription factor A, mitochondrial), a nuclear-encoded gene that is essential for mitochondrial gene transcription and mitochondrial DNA replication.**

Methods and Results: ***Tfam*** **inactivation by Nkx2.5^{Cre} caused mitochondrial dysfunction and embryonic lethal myocardial hypoplasia. *Tfam* inactivation was accompanied by elevated production of reactive oxygen species (ROS) and reduced cardiomyocyte proliferation. Mosaic embryonic *Tfam* inactivation confirmed that the block to cardiomyocyte proliferation was cell autonomous. Transcriptional profiling by RNA-seq demonstrated the activation of the DNA damage pathway. Pharmacological inhibition of ROS or the DNA damage response pathway restored cardiomyocyte proliferation in cultured fetal cardiomyocytes. Neonatal *Tfam* inactivation by AAV9-cTnT-Cre caused progressive, lethal dilated cardiomyopathy. Remarkably, postnatal *Tfam* inactivation and disruption of mitochondrial function did not impair cardiomyocyte maturation. Rather, it elevated ROS production, activated the DNA damage response pathway, and decreased cardiomyocyte proliferation. We identified a transient window during the first postnatal week when inhibition of ROS or the DNA damage response pathway ameliorated the detrimental effect of *Tfam* inactivation.**

Conclusions: **Mitochondrial dysfunction caused by *Tfam* inactivation induced ROS production, activated the DNA damage response, and caused cardiomyocyte cell cycle arrest, ultimately resulting in lethal cardiomyopathy. Normal mitochondrial function was not required for cardiomyocyte maturation. Pharmacological inhibition of ROS or DNA damage response pathways is a potential strategy to prevent cardiac dysfunction caused by some forms of mitochondrial dysfunction. (*Circ Res*. 2018;122:74-87. DOI: 10.1161/CIRCRESAHA.117.311349.)**

Key Words: cardiomyocyte maturation ■ cell cycle ■ mitochondria ■ reactive oxygen species ■ transcription factor

Mitochondria are a central hub of cellular metabolism and energy production. Mutations in genes encoded in both the nuclear and mitochondrial genomes can disrupt mitochondrial function, resulting in diseases with myriad manifestations, including cardiac hypertrophy, noncompaction, and failure.[1] Although the need for mitochondria to produce an adequate supply of energy is the most obvious link between mitochondrial diseases and heart failure, other metabolic derangements may be equally if not more important for muscle cell dysfunction.[2] Moreover, the mechanisms by which mitochondrial abnormalities cause aberrant cardiac morphogenesis, such as left ventricular noncompaction, are largely unknown. Greater understanding of the role of mitochondria in cardiac morphogenesis and maturation may provide insights into the pathogenesis of mitochondrial cardiomyopathies and identify productive therapeutic avenues to ameliorate the consequences of mitochondrial disease.

Editorial, see p 11
Meet the First Author, see p 3

Few studies have examined the role of mitochondria in governing cardiac development and maturation. Hom et al[3] implicated mitochondria, and specifically mitochondrial

Original received May 16, 2017; revision received September 29, 2017; accepted October 10, 2017. In September 2017, the average time from submission to first decision for all original research papers submitted to *Circulation Research* was 13 days.

From the Department of Cardiology, Boston Children's Hospital, MA (D.Z., Y.L., D.H.-W., V.B., S.G., Y.G., F.G., P.Z., Z.L., Q.M., J.L., D.-Z.W., W.T.P.); Hubei Collaborative Innovation Center for Green Transformation of Bio-Resources, Hubei Key Laboratory of Industrial Biotechnology, College of Life Sciences, Hubei University, Wuhan, China (D.Z.); Key Laboratory of Birth Defects and Related Diseases of Women and Children of MOE, Department of Pediatrics, West China Second University Hospital, Sichuan University, Chengdu, Sichuan (Y.L.); Physiology and Biophysics, Institute of Biological Sciences, Universidade Federal de Minas Gerais, Belo Horizonte, Brazil (S.G.); and Harvard Stem Cell Institute, Harvard University, Cambridge, MA (W.T.P.).

*These authors contributed equally to this article.

The online-only Data Supplement is available with this article at http://circres.ahajournals.org/lookup/suppl/doi:10.1161/CIRCRESAHA.117.311349/-/DC1.

Correspondence to Donghui Zhang, PhD, Hubei Key Laboratory of Industrial Biotechnology, College of Life Sciences, Hubei University, Wuhan 430062, China, E-mail dongh.zhang@hubu.edu.cn; or William T. Pu, MD, Department of Cardiology, Boston Children's Hospital, Enders 1254, 320 Longwood Ave, Boston, MA 02115, E-mail wpu@pulab.org

Novelty and Significance

What Is Known?

- Mutations in genes essential for mitochondrial function often affect cardiac morphogenesis and postnatal cardiac function.
- Postnatal cardiomyocyte maturation involves striking changes in both morphology and metabolism, which has led to the hypothesis that metabolic maturation is required for morphological maturation.
- The nuclear-encoded mitochondrial protein TFAM (mitochondrial transcription factor A) is required for mitochondrial gene expression and DNA replication.

What New Information Does This Article Contribute?

- Early stage inactivation of a conditional *Tfam* allele in cardiomyocytes caused lethal defects in cardiac development associated with reactive oxygen species (ROS)–induced cardiomyocyte cell cycle activity.
- Postnatal mitochondrial dysfunction induced by neonatal cardiomyocyte-selective *Tfam* inactivation likewise reduced neonatal cardiomyocyte proliferation and caused progressive heart failure.
- In this neonatal *Tfam* cardiomyocyte inactivation model, suppressing ROS or kinases responsible for the G2/M cell cycle checkpoint in the neonatal period delayed the progression of heart failure.
- Mosaic *Tfam* inactivation in neonatal cardiomyocytes did not have a cell-autonomous effect on their morphological maturation.

Gene mutations that impair mitochondrial function often disrupt cardiac morphogenesis and function, but the mechanistic links between mitochondria, cardiac morphogenesis, and heart failure are incompletely understood. Here, we study both fetal and neonatal inactivation of *Tfam*, which is required for mitochondrial gene expression and DNA replication. *Tfam* inactivation at either stage elevated ROS and activated the DNA damage response, resulting in reduced cardiomyocyte cell cycle activity. Suppressing ROS or blocking WEE kinase, required for the G2/M cell cycle checkpoint, restored cardiomyocyte cell cycle activity. In the neonatal *Tfam* inactivation model, ROS suppression or WEE kinase inhibition delayed the progression of heart failure. Using a mosaic *Tfam* inactivation approach, we further demonstrate that mitochondrial dysfunction caused by *Tfam* depletion did not affect postnatal cardiomyocyte morphological maturation. Together our data demonstrate that reduced cardiomyocyte cell cycle activity is 1 mechanism that links mitochondrial dysfunction to abnormal cardiac morphogenesis and function. In addition, our study points out that the neonatal period may offer a therapeutic window during which intervention can ameliorate later cardiac dysfunction.

Nonstandard Abbreviations and Acronyms

AAV	adeno-associated virus
E	embryonic day
MK	MK-1755
MT	mitoTEMPO
P	postnatal day
pH3	phosphohistone H3
Ppargc1α	peroxisome proliferator-activated receptor gamma coactivator 1-α
Ppargc1β	peroxisome proliferator-activated receptor gamma coactivator 1-β
ROS	reactive oxygen species
TFAM	mitochondrial transcription factor A
Tfam^{NK}	Tfam$^{fl/fl}$ inactivated by Nkx2-5^{Cre}
TUNEL	terminal deoxynucleotidyl transferase dUTP nick end labeling
T-tubule	transverse tubule

reactive oxygen species (ROS) signaling, in promoting fetal cardiomyocyte maturation. Cardiac ablation of both *Ppargc1α* (peroxisome proliferator-activated receptor gamma coactivator 1-α) and *Ppargc1β* (peroxisome proliferator-activated receptor gamma coactivator 1-β), nuclear transcriptional coactivators required for mitochondrial biogenesis and expression of nuclearly encoded mitochondrial genes, caused late gestational defects in cardiac function and cardiomyocyte maturation,[4] providing further evidence that mitochondria are required for normal cardiomyocyte maturation. On the other hand, cardiac-specific inactivation of genes encoding core components of the mitochondrial electron transport chain (eg, *Ndufs4*[5] or *Ndufs6*[6]) caused lethal postnatal cardiomyopathy but ostensibly did not impact embryonic survival or cardiac development.

TFAM (mitochondrial transcription factor A) is a nucleus-encoded protein that is required for mitochondrial DNA transcription.[7] Ablation of *Tfam* prevents expression of the 13 polypeptides encoded in the mitochondrial genome, all components of enzyme complexes required for oxidative phosphorylation. TFAM is also required to maintain mitochondrial DNA stability, both by stimulating its replication and by binding it to form nucleoids.[7] Although *Tfam* inactivation reduced mitochondrial number and mass, in some contexts, it elevated ROS production, likely as a result of electron transport chain impairment.[8] Conditional *Tfam* inactivation in cardiomyocytes by Myh6 (myosin heavy chain 6)-Cre[9] or MCK-Cre[10] was previously shown to cause lethal dilated cardiomyopathy. Survival to birth was reportedly normal, and most Tfam$^{fl/fl}$; Myh6-Cre neonates died in the first week. However, the effect on cardiac development or cardiomyocyte maturation was not investigated.

Here, we inactivated *Tfam* in cardiomyocytes to disrupt mitochondrial function and evaluate the consequences on cardiac development, cardiomyocyte maturation, and cardiac function. We found that *Tfam* inactivation in fetal cardiomyocytes severely impaired cardiomyocyte proliferation, associated with severe myocardial hypoplasia and fetal demise. Impaired cardiomyocyte proliferation was linked to ROS-mediated activation of the DNA damage response pathway. Postnatally, *Tfam* inactivation impaired neonatal cardiomyocyte proliferation but morphologically did not alter cardiomyocyte maturation. Cardiomyopathy caused by neonatal *Tfam* inactivation was ameliorated by the inhibition of ROS or the DNA damage response pathway, suggesting a potential therapeutic strategy for mitochondrial cardiomyopathies.

Methods

Detailed Methods are given in the Online Data Supplement.

Animal

All animal procedures were performed following protocols approved by the Institutional Animal Care and Use Committee of Boston Children's Hospital. Tfam$^{fl/fl}$, Nkx2-5$^{IRES\text{-}CRE/+}$, ROSA26^{CreERT2}, and Rosa26^{tdTomato} mice, and AAV9-TnT-Cre were described previously.[9,11–14] Adeno-associated virus (AAV) was injected subcutaneously at postnatal day 1 (P1) or P8 at 4.0×10^{10} vg/g (high dose) or 8.0×10^{9} vg/g (low dose).

Fetal Cardiomyocyte Culture

Embryonic day 15.5 (E15.5) cardiomyocytes were isolated using the Neomyt Kit (Cellutron, NC-6031). Adenovirus expressing Cre (Ad:Cre) or LacZ (Ad:LacZ) was added on day 1.

Mitochondrial function was measured using a Seahorses Biosciences XF96e analyzer.

Histology

Tissues were fixed in 4% paraformaldehyde, and 8 µm cryosections were immunostained using antibodies listed in the detailed Methods (Online Data Supplement). Apoptosis was measured using the terminal deoxynucleotidyl transferase dUTP nick end labeling (TUNEL) Assay Kit (Abcam, ab66108).

Adult Cardiomyocyte Characterization

Adult cardiomyocytes were isolated by Langendorff perfusion as described previously.[15] In situ transverse tubule (T-tubule) imaging was performed as described.[15] T-tubule organization was quantified using AutoTT.[15,16] Contraction of isolated ventricular cardiomyocytes was measured using an IonOptix system. Intracellular Ca^{2+} recordings were obtained by line scan imaging of cardiomyocytes loaded with Fluo-4 AM (Life Technologies).

RNA-Seq and Gene Expression

Polyadenylated RNA was isolated and converted into stranded RNA-seq libraries using Script-Seq v2 (Illumina). Real-time PCR was performed using primer sequences listed in Online Table I.

Statistics

Unless otherwise specified, bar graphs present data as mean±SD. Significance of intergroup differences was tested using Student *t* test or the Mann–Whitney test as indicated (SPSS 20.0).

Results

Cardiac-Specific Deletion of Tfam Causes Embryonic Lethality at E15.5

To disrupt mitochondrial function in fetal cardiomyocytes early in cardiac development, we used Nkx2.5$^{IRES\text{-}Cre}$ to inactivate a conditional *Tfam* allele[9] (Tfam$^{fl/fl}$; Nkx2.5$^{IRES\text{-}Cre/+}$ [Tfam^{NK}]). Tfam$^{fl/+}$; Nkx2-5$^{IRES\text{-}Cre/+}$ littermates were used as controls. We analyzed embryos from E13.5 to birth and found that Tfam^{NK} mutants were present at a normal Mendelian ratio at E13.5 and E15.5, but no viable mutants were recovered at E16.5 or birth (Figure 1A). At E15.5, Tfam^{NK} mutants had strikingly thin myocardial walls (Figure 1B). E13.5 hearts likewise showed thinner myocardial walls (Online Figure IA). Quantitative RT-PCR demonstrated reduction of *Tfam* mRNA in Tfam^{NK} mutants (Figure 1C), and TFAM immunostaining confirmed protein depletion (Figure 1D). Immunoblotting also demonstrated the reduction of TFAM and ATP5B, a nuclear-encoded mitochondrial protein, in Tfam^{NK} mutants (Online Figure IB). Furthermore, mitochondrial DNA copy number relative to nuclear DNA was reduced by 9.2-fold compared with control (Online Figure IC).

Tfam Is Essential for Mitochondrial Morphogenesis and Function

To investigate the effect of *Tfam* inactivation on mitochondria, we analyzed mitochondrial morphology in E15.5 hearts

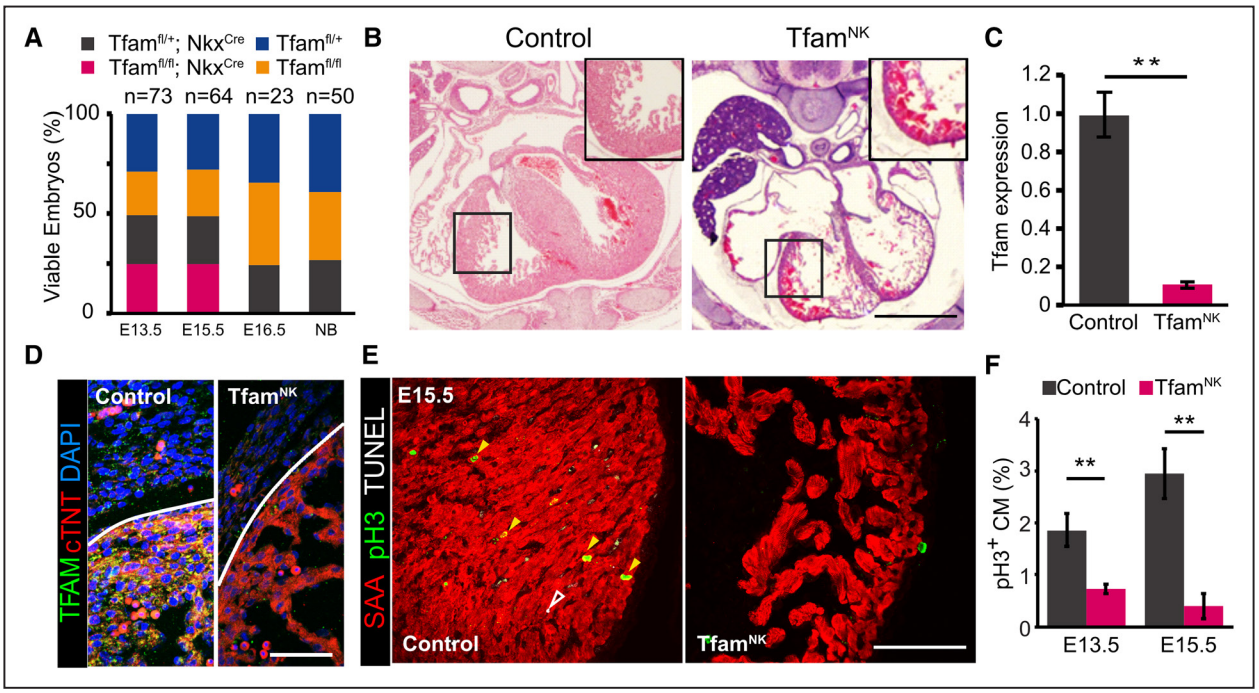

Figure 1. Abnormal development of Tfam^{NK} (Tfamfl/fl; Nkx2.5IRES-Cre/+) heart. A, Distribution of genotypes at indicated gestational ages. **B**, Morphology of Tfam^{NK} and control heart at embryonic day 15.5 (E15.5), shown in H&E (hematoxylin and eosin) stained transverse sections. Boxed areas are enlarged in the insets. Bar, 200 µm. **C**, Relative *Tfam* expression in control and Tfam^{NK} embryos by qPCR. n=6. **D**, Representative E15.5 heart sections stained for TFAM, demonstrating reduced immunoreactivity in Tfam^{NK} heart. Bar, 50 µm. **E**, Representative E15.5 heart sections stained for cardiomyocyte (CM) marker sarcomeric α-actinin (SAA), M-phase marker phosphohistone H3 (pH3), and apoptosis marker terminal deoxynucleotidyl transferase dUTP nick end labeling (TUNEL). Bar, 100 µm. Filled yellow arrowheads, pH3^{+} CM. Open white arrowhead, TUNEL^{+} CM. **F**, Quantification of the frequency of pH3^{+} CMs. n=6. *t* test: **, $P<0.01$. NB indicates newborn; and Tfam, mitochondrial transcription factor A.

by electron microscopy. Tfam^{NK} mitochondria had abnormal morphology and organization (Online Figure IIA). Cristae within mitochondria also appeared more sparse and irregular in Tfam^{NK} cardiomyocytes. Quantitative analysis showed that average mitochondrial size was lower in the Tfam^{NK} cardiomyocytes (Online Figure IIB). The mitochondrial area fraction was also reduced in Tfam^{NK} cardiomyocytes (Online Figure IIC). These data indicate that *Tfam* inactivation disrupts mitochondrial biogenesis and morphology.

We next assessed the effect of *Tfam* ablation on mitochondrial function. We cultured cardiomyocytes dissociated from E15.5 Tfam$^{fl/fl}$; Rosa26^{tdTomato} hearts. To deplete *Tfam* and activate the Cre-dependent tdTomato reporter, we transduced the cultured cardiomyocytes with adenovirus expressing Cre (Ad:Cre), resulting in the activation of tdTomato in >90% of cardiomyocytes. Ad:LacZ transduced cardiomyocytes served as controls. Immunostaining 48 hours after virus treatment showed markedly reduced TFAM immunoreactivity in tdTomato^{+} Cre-recombined cells, consistent with effective gene inactivation (Online Figure III). Furthermore, staining for mitochondrial marker ATP5B demonstrated decreased mitochondrial abundance (Online Figure III) and perinuclear predominance, in contrast to control cardiomyocytes in which mitochondria were distributed throughout the cytoplasm (Online Figure III).

Having established an efficient system for in vitro *Tfam* ablation in fetal cardiomyocytes, we next assessed the effect on mitochondrial function using a microfluidic extracellular flux analyzer (Online Figure IVA through IVC). *Tfam* inactivation increased basal respiration, which was attributable to greater F1F0-ATPase–linked respiration and to a lesser extent on increased proton leak (Online Figure IVA through IVC). Moreover, maximal respiratory rate was significantly lower in *Tfam*-deleted cardiomyocytes, indicative of reduced maximal electron transport chain activity (Online Figure IVA through IVC). Although *Tfam*-deficient cardiomyocytes exhibited impaired respiration, their extracellular acidification rate, a measure of glycolytic activity, was elevated (Online Figure IVD and IVE).

Functional mitochondria have hyperpolarized inner mitochondrial membranes. We assessed mitochondrial membrane potential with JC-1, which stains normal, hyperpolarized mitochondria red and impaired, depolarized mitochondria green. Confocal imaging demonstrated increased green and decreased red staining of mitochondria in Tfam$^{fl/fl}$ cardiomyocytes treated with Ad:Cre, indicative of mitochondrial depolarization (Online Figure VA). Quantitative data obtained by flow cytometry confirmed decreased red/green fluorescence ratio in *Tfam*-depleted cardiomyocytes (Online Figure VB). Indeed, the red/green ratio in *Tfam*-deficient cardiomyocytes approached the level observed when cardiomyocytes were treated with carbonyl cyanide 4-(trifluoromethoxy)phenylhydrazone (also known as FCCP), which abrogates mitochondrial membrane potential (Online Figure VB). These data demonstrate that *Tfam* inactivation depolarizes mitochondria.

To assess the effect of *Tfam* knockout on cellular energy reserves, we measured the ADP/ATP ratio in both cardiomyocytes freshly dissociated from fetal hearts and cultured cardiomyocytes. In E15.5 cardiomyocytes and cultured cardiomyocytes 3 and 7 days after Ad:Cre treatment, ADP/ATP ratio was lower in *Tfam*-deficient samples (Online Figure VI). This suggests that *Tfam*-deficient cardiomyocytes surprisingly did not have depletion of energy stores, potentially because of increased glycolytic activity.

Tfam Is Required Cell Autonomously for Fetal Cardiomyocyte Proliferation

A major effect of *Tfam* inactivation on fetal heart development was myocardial hypoplasia (Figure 1B). To assess the underlying cellular mechanism, we analyzed cardiomyocyte proliferation and apoptosis at E13.5 and E15.5. At both stages, the fraction of cardiomyocytes expressing the M-phase marker phosphohistone H3 (pH3) was markedly and significantly decreased in Tfam^{NK}, indicative of depressed cardiomyocyte proliferation (Figure 1E and 1F). Measurement of Ki67 further confirmed reduced cardiomyocyte proliferation at E15.5 (Online Figure VIIA and VIIB). TUNEL staining showed that TUNEL^{+} cardiomyocytes were significantly more frequent in Tfam^{NK} hearts at E13.5 but not E15.5 (Figure 1E; Online Figure VIIC). However, in both groups, TUNEL^{+} cardiomyocytes were infrequent. Together these data suggest that myocardial hypoplasia was because of both reduced cardiomyocyte proliferation and increased cardiomyocyte apoptosis, with the change in proliferation likely making a relatively larger contribution.

We used 2 independent approaches to assess whether decreased proliferation was a direct, cell-autonomous effect of *Tfam* inactivation, as opposed to a secondary or indirect consequence of impaired embryo health or myocardial dysfunction. First, we used a tamoxifen-inducible Cre allele (Rosa26^{CreERT2}) and a low dose of tamoxifen to inactivate *Tfam* in a minor fraction of cells (Online Figure VIIIA). In pilot experiments, we titrated the amount of tamoxifen administered at E8.5 so that CreERT2 activated the Cre-dependent Rosa26^{tdTomato} reporter in ≈30% of cardiomyocytes by E15.5 (Online Figure VIIIB and VIIIC). When this tamoxifen dose was administered to Tfam$^{fl/fl}$; Rosa26$^{CreERT2/tdTomato}$ embryos, by immunostaining, 80% of tdTomato^{+} cardiomyocytes lacked detectable TFAM immunoreactivity (Online Figure VIIID and VIIIE), indicating that the large majority of tdTomato^{+} cardiomyocytes lack TFAM. We then analyzed tdTomato^{+} and tdTomato^{-} cells from tamoxifen-treated Tfam$^{fl/fl}$; Rosa26$^{CreERT2/tdTomato}$ or Tfam$^{fl/+}$; Rosa26$^{CreERT2/tdTomato}$ for cell cycle activity, as measured by pH3 staining (Figure 2A). As expected, in tdTomato^{-} cells, which were not recombined by CreERT2, there was no significant difference in the frequency of pH3^{+} cardiomyocytes (Figure 2B). In contrast, in tdTomato^{+} cells, which were recombined by CreERT2, pH3^{+} cardiomyocytes from Tfam$^{fl/fl}$ embryos were significantly less frequent than from Tfam$^{fl/+}$ littermates (Figure 2B). This genetic mosaic analysis demonstrated that *Tfam* required cell autonomously for normal cardiomyocyte proliferation. This result makes potential confounding effects from poor cardiac function or low embryo viability less likely because the embryos were phenotypically normal as a result of the low fraction of cells that were mutated.

Second, we studied the effect of *Tfam* inactivation on cardiomyocyte proliferation in cultured fetal cardiomyocytes. We measured cardiomyocyte proliferation using both uptake

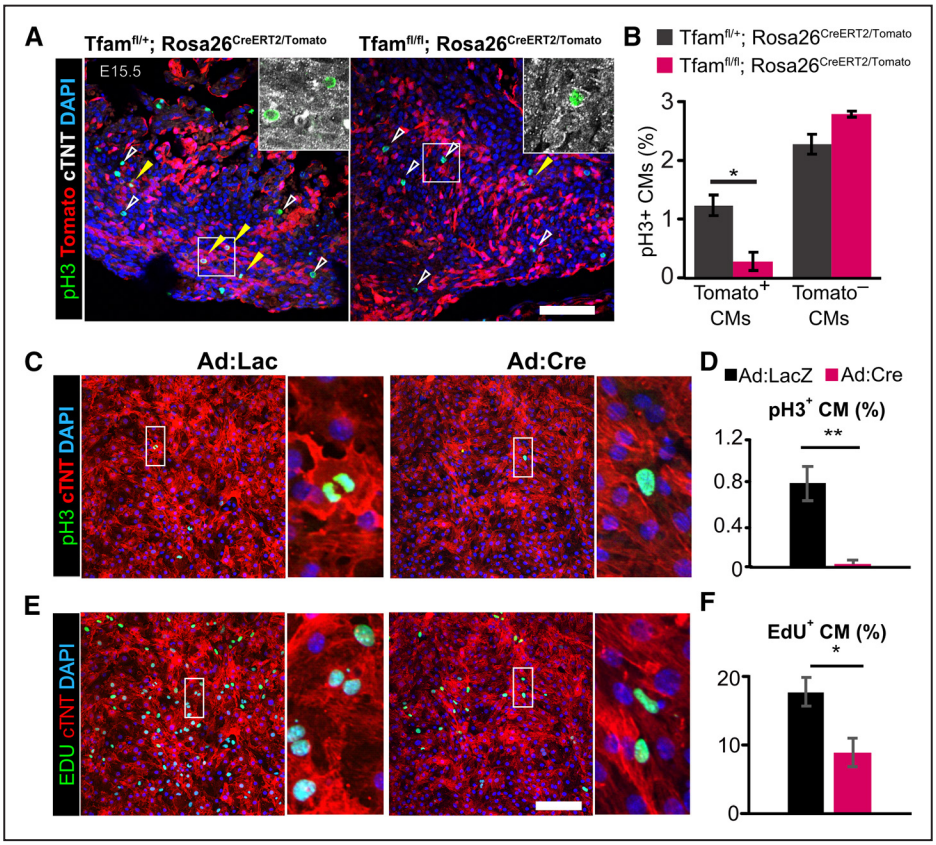

Figure 2. *Tfam* (mitochondrial transcription factor A) inactivation cell autonomously reduced cardiomyocyte (CM) proliferation. **A**, Representative images of embryonic day 15.5 (E15.5) heart sections stained for CM marker (cardiac Troponin T, cTNT), Cre marker (Tomato), and M-phase marker (phosphohistone H3 [pH3]). Insets show magnification of boxed regions with cTNT staining indicated in white. Filled yellow arrowheads, pH3$^+$, tdTomato$^+$ CMs. Open white arrowheads, pH3$^+$, tdTomato$^-$ cells. Bar, 100 μm. Boxed regions are magnified in inset with cTNT staining shown in white. **B**, Quantification of the percentage of pH3$^+$ CMs from staining described in (**A**). Three sections were stained and imaged per heart, and 5 independent hearts were studied. **C**–**F**, CMs cultured as in **C** and exposed to 5-ethynyl-2′-deoxyuridine (EdU) for 24 hours were stained for pH3 or EdU. Representative confocal images are shown in **C** and **E**, and boxed regions are magnified in insets on the **right**. Bar, 100 μm. Results are quantified in **D** and **F**. n=6. *P<0.05. **P<0.01.

of the nucleotide analog 5-ethynyl-2′-deoxyuridine (passage through S phase) and immunostaining for pH3 (M phase). Both measures of cell cycle activity were reduced in *Tfam*-depleted cardiomyocytes (Figure 2C through 2F). Because the intrauterine environment has lower oxygen tension, we repeated these experiments under hypoxic conditions (7% oxygen). Cell cycle activity of both control and *Tfam*-depleted groups was higher in hypoxia compared with normoxia, consistent

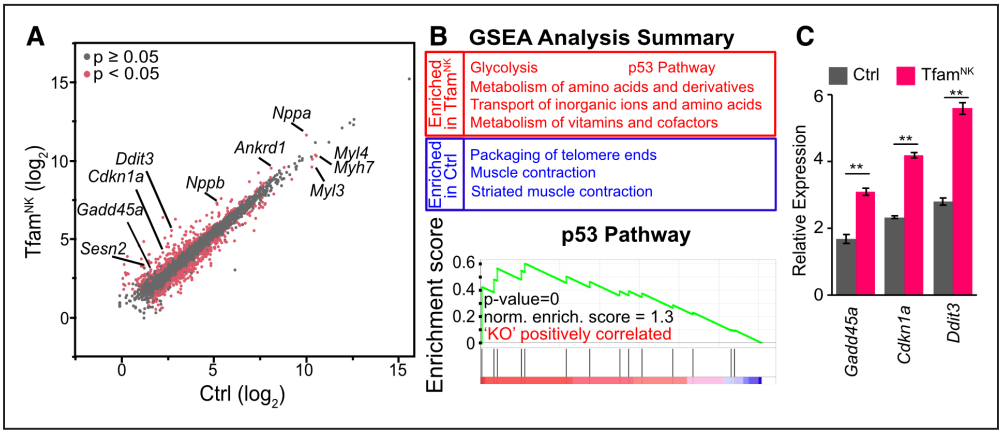

Figure 3. RNA-seq analysis of *Tfam* (mitochondrial transcription factor A) inactivation in fetal heart. RNA-seq was performed on Tfam^{NK} (Tfam$^{fl/fl}$; Nkx2.5$^{IRES\text{-}Cre/+}$) and control hearts at embryonic day 13.5 (E13.5; n=3 per group). **A**, Scatterplot of gene expression in Tfam^{NK} and control. Selected differentially expressed genes are labeled. **B**, Summary of Gene Set Enrichment Analysis (GSEA) for RNA-seq data. Selected pathways significantly enriched in Tfam^{NK} or control are listed. Leading edge analysis of the p53 pathway is shown. **C**, Relative expression of selected genes differentially expressed in p53 pathway based on the RNA-seq results. **P<0.01. pH3 indicates phosphohistone H3.

with recent studies,[17] but the proliferation rate of hypoxic *Tfam*-depleted cardiomyocytes remained lower than hypoxic controls (Online Figure IX).

Collectively, these data demonstrate that *Tfam* inactivation cell autonomously reduces fetal cardiomyocyte proliferation.

Tfam Ablation Elevates ROS Levels and Activates DNA Damage Response Pathways

To further assess the mechanisms by which *Tfam* ablation inhibits cell cycle activity, we performed RNA-seq on Tfam^{NK} and control hearts (n=3 biological replicates per group, 5 hearts per replicate). Hearts were collected at E13.5, before the onset of severe morphological abnormalities. There were 346 upregulated and 449 downregulated genes (adjusted *P* value <0.05; Figure 3A). Gene set enrichment analysis[18] of the RNA-seq data (Figure 3B) showed that the mutant is enriched for terms related to glycolysis and metabolism, consistent with the central role of mitochondria in cellular metabolism. Muscle contraction gene sets were downregulated in mutants, suggesting a link between mitochondrial function and expression of contractile genes. Interestingly, DNA damage response terms, most notably the p53 DNA damage response pathway, were enriched in Tfam^{NK}. Key upregulated genes in this pathway included *Cdkn1a* (encoding the cell cycle inhibitor p21), *Gadd45a*, a gene induced by the DNA damage response pathway, and *Ddit3*, a gene that mediates cell cycle arrest and that is induced by DNA damage (Figure 3C).

At birth, exposure to increased oxygen tension results in greater mitochondrial ROS production in normal cardiomyocytes, and this has been linked to cell cycle exit through the activation of DNA damage response pathways.[17] Elevated ROS and activation of the p53 pathway have also been implicated in damage to telomeres, and the gene set Packaging of telomere ends was downregulated in Tfam^{NK}. Therefore, we hypothesized that elevated ROS production by *Tfam*-depleted cells[19] activates DNA damage response pathways, resulting in cell cycle exit.

The effect of *Tfam* ablation on ROS levels is cell context dependent: *Tfam* inactivation elevated ROS in adipocytes[8] but reduced ROS in keratinocytes.[19] Therefore, as a first step toward testing this hypothesis, we evaluated the effect of *Tfam* ablation on fetal cardiomyocyte ROS levels. Tfam^{NK} heart sections had elevated levels of 4-hydroxynonenal, a product of lipid peroxidation by ROS, at E13.5 and E15.5 (Figure 4A and 4B). In cultured E15.5 Tfam$^{fl/fl}$; Rosa26^{tdTomato} cardiomyocytes, we measured cellular ROS levels using CellRox, a fluorogenic live cell ROS probe. Positive control cells treated with 50 µmol/L H_2O_2 exhibited high CellRox fluorescence, as expected (Figure 4C, left). In Ad:LacZ-treated cardiomyocytes, most cells had low CellRox signal, consistent with low ROS levels (Figure 4C, middle). In contrast, tdTomato$^+$, Ad:Cre-transduced Tfam$^{fl/fl}$; Rosa26^{tdTomato} cardiomyocytes exhibited markedly increased CellRox fluorescence (Figure 4C, right, upper right quadrant), whereas there the frequency of

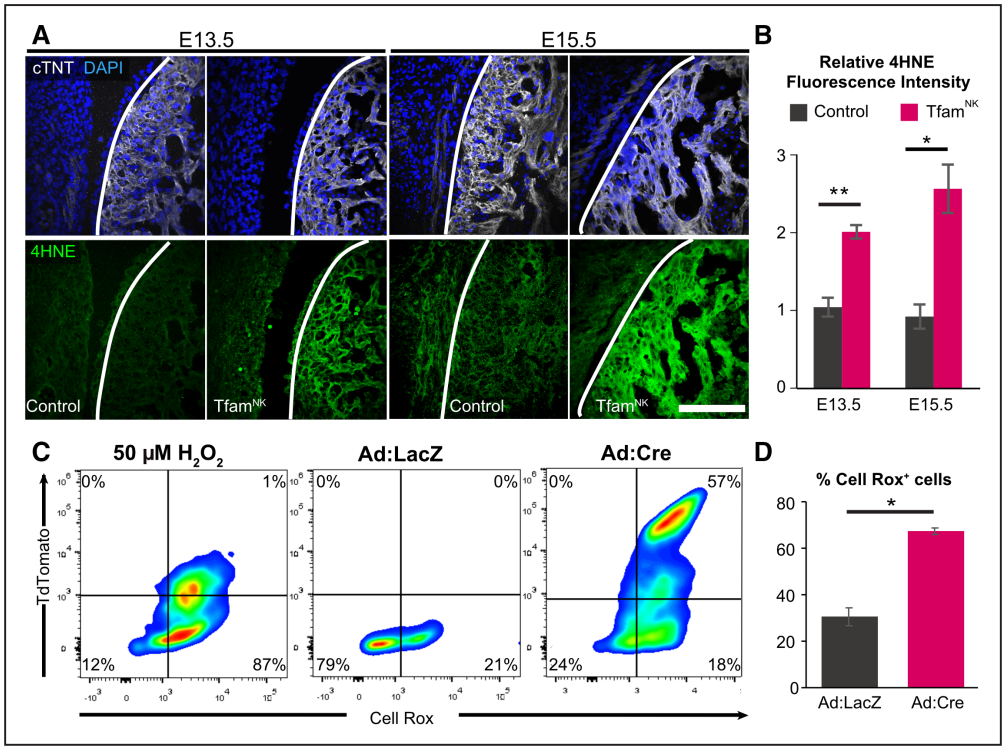

Figure 4. *Tfam* (mitochondrial transcription factor A) inactivation elevates cardiomyocyte (CM) reactive oxygen species (ROS) levels. A, Representative control and Tfam^{NK} (Tfam$^{fl/fl}$; Nkx2.5$^{IRES\text{-}Cre/+}$) tissue sections stained for lipid peroxidation product 4-hydroxynonenal (4HNE), CM marker (cTNT), and DAPI on tissue sections at embryonic day 13.5 (E13.5) and E15.5. **B**, Quantitative comparison of 4HNE staining intensity between control and Tfam^{NK} heart sections. Three sections were stained and imaged per heart, and 4 independent hearts were studied. **C**, Cultured Tfam$^{fl/fl}$; Rosa26^{tdTomato} E15.5 CMs were treated with H_2O_2 (positive control, **left**), Ad:LacZ (**middle**), and Ad:Cre (**right**). The fraction of CellRox$^+$-positive cells was measured by FACS (fluorescence-activated cell sorting). **D**, Quantification of CellRox$^+$ cells between Ad:LacZ- and Ad:Cre-treated groups. Because LacZ control cells did not activate the Tomato reporter, we compared total CellRox$^+$ cells between groups. *P<0.05. **P<0.01.

CellRox-positive, tdTomato$^-$ cells was not substantially affected (Figure 4C, right, lower right quadrant). Quantitative analysis across replicates confirmed that *Tfam* ablation markedly increased cardiomyocyte ROS production (Figure 4D). To determine whether the excess ROS originated from mitochondria, we used the mitochondrially targeted ROS fluorescent probe Mitosox. *Tfam*-depleted cardiomyocytes exhibited greater Mitosox fluorescent intensity than control cardiomyocytes (Online Figure X), supporting elevated mitochondrial ROS production in these cells.

Together these data indicate that mitochondria in *Tfam*-depleted cardiomyocytes produce excess ROS by impairing electron transport chain function.[20] Elevation of ROS and the transcriptomic signature of activated DNA damage response in *Tfam*-deficient cardiomyocytes suggested the hypothesis that ROS activation of the DNA damage response reduces their cell cycle activity.

Rescue of Cell Cycle Activity of Tfam-Deficient Cardiomyocytes by ROS or WEE1 Kinase Inhibition

DNA oxidation by ROS triggers phosphorylation of histone H2A.X (γH2A.X), which accumulates at sites of damage and serves as a platform that activates the DNA damage checkpoint to progression from G2 to M phase of the cell cycle.[21] In cultured fetal cardiomyocytes, *Tfam* ablation induced increased γH2A.X (Online Figure XIA and XIB), consistent with ROS-mediated DNA damage and activation of DNA damage response pathways. In hypoxic culture conditions (7% O_2), overall frequency of γH2A.X cardiomyocytes was lower, but *Tfam*-depleted cardiomyocytes continued to have elevated γH2A.X compared with control (Online Figure XIC and XID).

To test the hypothesis that elevated ROS production from *Tfam*-deficient cardiomyocytes contributed to reduced cardiomyocyte proliferation, we treated cultured cardiomyocytes with the mitochondrially targeted ROS scavenger mitoTEMPO (MT). MT normalized γH2A.X levels in *Tfam*-depleted cultured fetal cardiomyocytes (Figure 5A and 5B). This effect of MT was accompanied by increased cell cycle activity, as measured by Ki67 staining (Figure 5C and 5D). These data suggest that elevated ROS in *Tfam*-depleted cardiomyocytes activates the DNA damage response to reduce cardiomyocyte cell cycle activity.

Cell cycle progression through the G2/M checkpoint depends on CDC25-mediated dephosphorylation of CDK1 at tyrosine-15.[22] WEE1 kinase counterbalances CDC25 by phosphorylating this residue. Activation of DNA damage response pathways inhibits CDC25 activity and thereby prevents progression through the G2/M checkpoint. We reasoned that DNA damage–mediated cell cycle inhibition could be ameliorated by inhibiting WEE1 kinase.[17] Treatment of *Tfam*-deficient, cultured fetal cardiomyocytes with MK-1755 (MK), a selective WEE1 kinase inhibitor, increased cell cycle activity, as measured by Ki67 staining (Figure 5C and 5D). Remarkably, MK-treated, *Tfam*-deficient cardiomyocytes had cell cycle activity that was not significantly different from

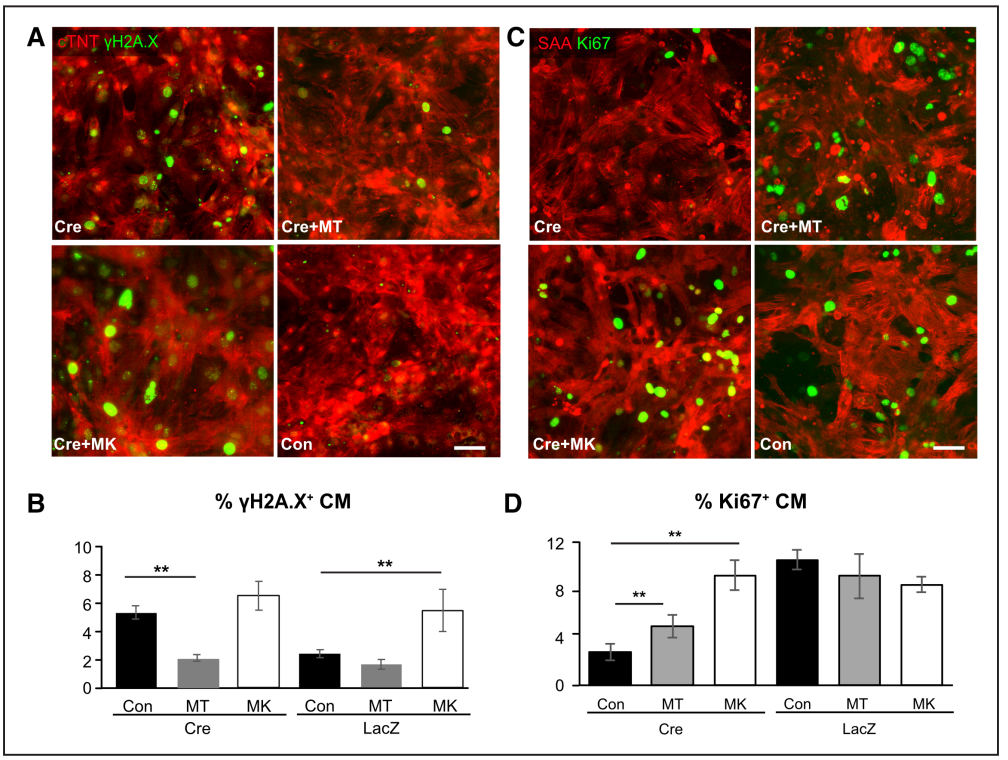

Figure 5. Rescue of cell cycle activity of *Tfam* (mitochondrial transcription factor A)-deficient cardiomyocytes (CMs) by reactive oxygen species (ROS) or WEE1 kinase inhibition. Cultured Tfam$^{fl/fl}$; Rosa26^{tdTomato} embryonic day 15.5 (E15.5) CMs were treated with Ad:Cre on the first day after seeding. Then MitoTEMPO (MT) or MK-1775 (MK) were added, and CMs were fixed and stained on the fifth day. **A**, Representative images of CMs treated with Cre, Cre+MT, Cre+MK, or LacZ (control, Con) and stained for γH2A.X and a CM marker (cardiac troponin T [cTNT]). Bar, 100 μm. **B**, Quantification of the percentage of γH2AX$^+$ CMs in (**A**). **C**, Representative images of CMs treated with Cre, Cre+MT, Cre+MK, or LacZ (Con) and stained for Ki67 and a CM marker (sarcomeric α-actinin [SAA]). Bar, 100 μm. **D**, Quantification of the percentage of Ki67$^+$-positive CMs in (**B**). *t* test: **P*<0.05. ***P*<0.01.

control cardiomyocytes. MK did not reduce γH2A.X levels in *Tfam*-deficient cardiomyocytes (Figure 5A and 5B), consistent with WEE1 kinase inhibition acting distal to this DNA damage signal.

Collectively, these data indicate that *Tfam* deficiency causes ROS-mediated DNA damage, which inhibits cardiomyocyte cell cycle activity through the activation of the G2/M checkpoint. ROS scavenging or WEE1 kinase inhibition rescues cardiomyocyte proliferation by reducing ROS or by relieving G2/M checkpoint cell cycle inhibition.

Inhibition of ROS-Activated DNA Damage Response Mitochondrial Rescues Cardiomyopathy In Vivo

To determine whether ROS suppression or WEE1 kinase inhibition protects cardiomyocyte proliferation from *Tfam* depletion in vivo, we developed and studied a model of neonatal *Tfam* deficiency because neonates are more accessible to interventions than embryos. This model is also more relevant to clinical scenarios of mitochondrial abnormalities, which typically present postnatally. $Tfam^{fl/fl}$; $Rosa26^{tdTomato/+}$ mice were treated with AAV9-cTNT-Cre (AAV9-Cre), in which cardiotropic adeno-associated virus 9 expresses Cre from the cardiac troponin T promoter.[14] At P0, we delivered 2 different doses of AAV9-cTNT-Cre (AAV9-Cre; 4×10^{10} vg or 8×10^{9} vg), referred to as high and low groups, respectively) to $Tfam^{fl/fl}$; $Rosa26^{tdTomato}$ mice (Figure 6A). Control mice with the genotype $Tfam^{fl/+}$; $Rosa26^{tdTomato}$ were treated with AAV9-Cre at the high dose. Three days after AAV treatment, ≈55% and 30% of cardiomyocytes expressed the tdTomato Cre–dependent reporter (Figure 6B; Online Figure XIIA). To confirm that AAV9-Cre effectively inactivates *Tfam* in $Tfam^{fl/fl}$; $Rosa26^{tdTomato}$ mice, we performed immunostaining on dissociated cardiomyocytes. We observed reduced TFAM immunoreactivity in $tdTomato^{+}$ cardiomyocytes (Figure 6C; Online Figure XIIB). We confirmed elevated levels of 8-oxoguanine, DNA damage induced by ROS, as well as increased 4-hydroxynonenal, P21 cell cycle inhibitor, WEE1 kinase, and γH2A.X in *Tfam*-deficient cardiomyocytes (Online Figure XIIC and XIID).

Mice were followed by serial echocardiography until 8 weeks of age. Consistent with prior cardiac knockout of *Tfam* using Myh6-Cre,[9] high-dose mice with a greater fraction of cardiomyocyte transduction developed progressive ventricular dysfunction and dilatation, as measured by echocardiography (Figure 6D and 6E). In contrast, the low-dose group had heart function that was not distinguishable from control (Figure 6D and 6E). These data show that *Tfam* inactivation in a large fraction of cardiomyocytes causes progressive cardiomyopathy, whereas its inactivation in a small fraction of cardiomyocytes is well tolerated and does not cause organ-level evidence of dysfunction.

Murine cardiomyocytes continue to proliferate until about P7, by which time they largely exit the cell cycle.[23,24] We hypothesized that *Tfam* ablation during this time period contributed to heart dysfunction by impairing cell cycle activity and that this effect of *Tfam* ablation could be ameliorated by either ROS or WEE1 kinase inhibition. To test this hypothesis, mice were treated with AAV9-Cre at the high dose and also with MT (ROS scavenger), MK (WEE1 inhibitor), or vehicle for the first postnatal week (Figure 6F). Remarkably, treatment with either MT or MK during the first postnatal week, when cardiomyocytes retain proliferative competence, ameliorated ventricular dysfunction at 8 weeks (Figure 6F).

We further tested this hypothesis using 2 independent approaches. In 1 approach, we treated a second cohort of mice with MT or MK in the second postnatal week (Figure 6G). Delaying therapy to this period outside of the period of cardiomyocyte proliferative competence resulted in it being ineffective. In a second approach, we asked whether inactivation of *Tfam* after cardiomyocytes lose proliferative competence has a less deleterious effect than when it is inactivated during active cardiomyocyte proliferation. $Tfam^{fl/fl}$; $Rosa26^{tdTomato}$ and $Tfam^{fl/+}$; $Rosa26^{tdTomato}$ mice at P8, and $Tfam^{fl/fl}$; $Rosa26^{tdTomato}$ mice at P1, were injected with the same weight-adjusted dose of AAV9-Cre. Serial echocardiography confirmed progressive, severe systolic dysfunction caused by AAV9-Cre delivery at P1 (Online Figure XIIIA). In comparison, AAV9-Cre delivery at P8 caused relatively less severe systolic dysfunction (Online Figure XIIIA). Together, these data suggest that impaired cardiomyocyte proliferation contributes to the progressive cardiomyopathy caused by neonatal *Tfam* knockout. Furthermore, the data point to a limited therapeutic window that corresponds to the time when cardiomyocytes are actively cycling.

We investigated the mechanisms underlying the response to MT and MK during the first postnatal week. Western blotting for TFAM or ATP5B indicated that MT and MK did not reduce the extent of TFAM or mitochondrial depletion (Online Figure XIVA). MT and MK likewise did not rescue expression of *mt-Atp6*, *mt-Nd1*, or *mt-Co1* genes encoded by the mitochondrial genome that require TFAM for transcription (Online Figure XIVB). We assessed neonatal cardiomyocyte proliferation at P5 by immunostaining tissue sections for Ki67 (Figure 6H and 6I) or pH3 (Online Figure XIVC and XIVD). Consistent with the results from cultured fetal cardiomyocytes, *Tfam* ablation strongly reduced neonatal cardiomyocyte proliferation (Figure 6H and 6I, Cre+Veh group). Treatment with MT increased cell cycle activity of Cre-recombined cardiomyocytes (Figure 6H and 6I, Cre+MT versus Cre+Veh in $tdTomato^{+}$ cardiomyocytes; Online Figure XIVC and XIVD). Interestingly, MT also increased cell cycle activity of non-recombined ($tdTomato^{-}$) cardiomyocytes (Figure 6H and 6I, Cre+MT versus Cr+Veh in $tdTomato^{-}$ cardiomyocytes), in keeping with reports that physiological increases in ROS during the neonatal period promote cell cycle exit.[17] WEE1 inhibition with MK did not enhance cell cycle activity of $tdTomato^{-}$ cardiomyocytes, but it strongly increased cell cycle activity of $tdTomato^{+}$ cardiomyocytes, restoring the $Ki67^{+}$ cardiomyocytes to levels comparable to $tdTomato^{-}$ controls (Figure 6H). These data indicate that MT and MK treatments inhibit ROS and DNA damage to rescue proliferation without ameliorating the effect of *Tfam* ablation on mitochondrial abundance or gene expression.

This result was corroborated by an independent approach. The dose of AAV9-Cre that we administered created a genetic mosaic in which $tdTomato^{+}$ cardiomyocytes lack Tfam and $tdTomato^{-}$ cardiomyocytes are replete in Tfam. Therefore, the fraction of $tdTomato^{+}$ cardiomyocytes is an independent

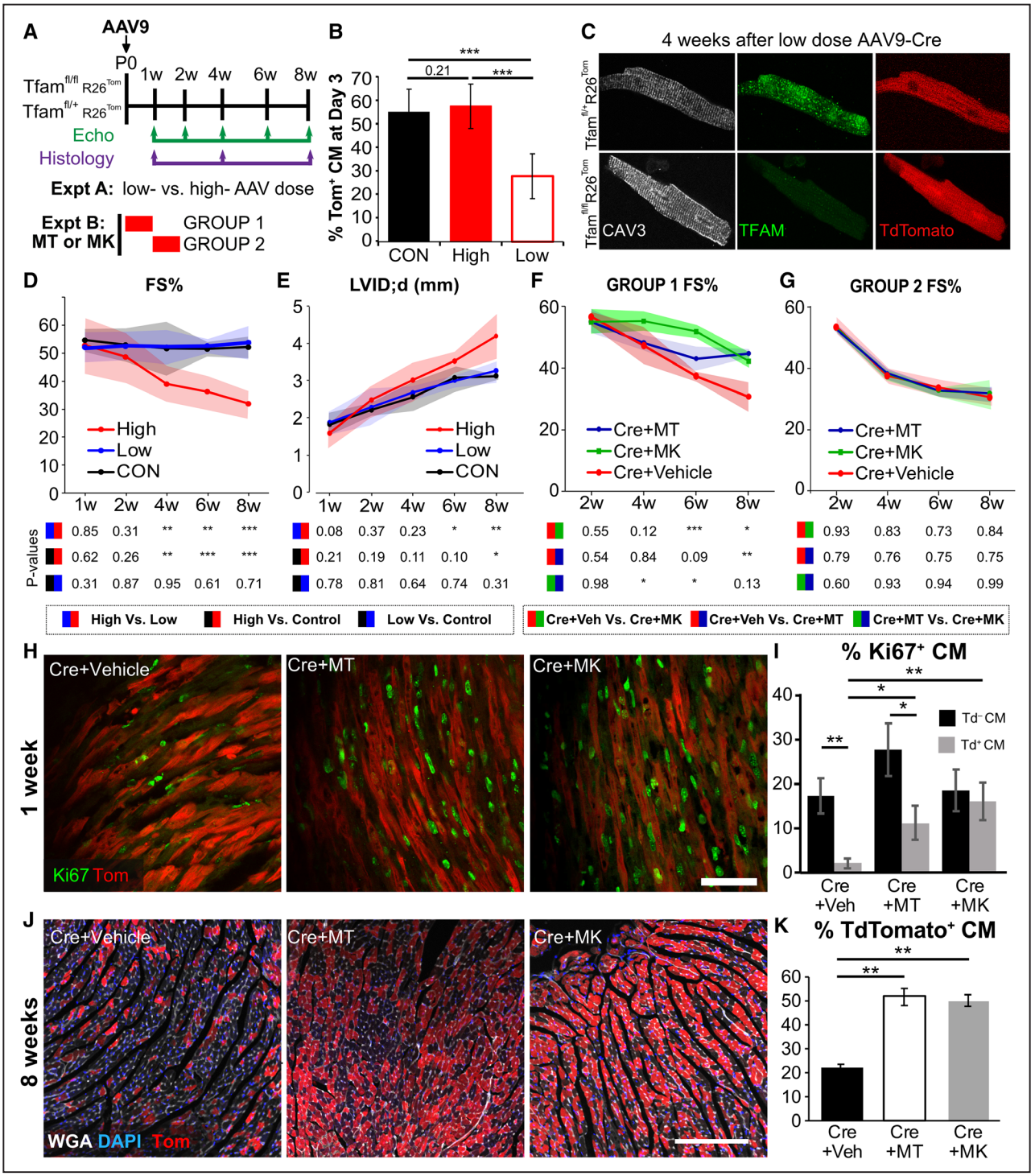

Figure 6. Inhibition of reactive oxygen species (ROS)–activated DNA damage response ameliorates cardiomyopathy in vivo. A, Experimental set-up and timeline. AAV9-Cre was injected at postnatal day 0 (P0). Experiment A examined the effect of AAV dose. Experiment B examined the effect of treatment with MitoTEMPO (MT) or MK-1775 (MK) during either the first or second postnatal week (groups 1 and 2, respectively). Echocardiography and tissue analyses were performed at the indicated times. **B**, The percentage of tdTomato+ cardiomyocytes (CMs) observed after AAV9-Cre injected. Tfam$^{fl/fl}$; Rosa26^{tdTomato} mice were treated with high- or low-dose AAV9-Cre, whereas Tfam$^{fl/+}$; Rosa26^{tdTomato} mice were treated with high dose (CON). **C**, Representative images of P28 CMs isolated from Tfam$^{fl/+}$; Rosa26^{tdTomato} or Tfam$^{fl/fl}$; Rosa26^{tdTomato} mice and control mice treated with AAV9-Cre at P0. CMs are stained for TFAM and CAV3 (caveolin 3), a transverse tubule (T-tubule) marker. **D**, **E**, Echocardiographic parameters from CON, low-dose, and high-dose mice. Shaded regions indicate standard error of the mean at each time point. **F**, **G**, Effect of MT or MK treatment on heart function when given in postnatal week 1 (group 1) or 2 (group 2). **H**, **I**, Representative heart tissue sections (**H**) stained for Ki67 at P5 after treatment with Cre+Vehicle, Cre+MT, or Cre+MK. Quantification of the percentage of Ki67+ CMs is shown in **I**. n=4. Bar, 50 μm. **J**, **K**, Representative heart tissue sections (**J**) from Cre+Vehicle-, Cre+MT-, or Cre+MK-treated mice. Sections were stained for WGA (wheat germ agglutinin) and DAPI and imaged for endogenous tdTomato fluorescence at 8 weeks. Bar, 200 μm. Quantification of the percentage of tdTomato+ CMs is shown in **K**. n=4. *t* test: **P*<0.05. ***P*<0.01. AAV indicates adeno-associated virus; FS, fraction shortening; LVID;d, left ventricular internal diameter at end diastole; and TFAM, mitochondrial transcription factor A.

measure of the relative proliferation of these populations. In heart sections from mice treated with AAV9-Cre at P0 and analyzed at 8 weeks of age, the tdTomato$^+$ cardiomyocyte fraction was lowest in the Cre group and significantly higher in both the Cre+MT and Cre+MK groups (Figure 6J and 6K), consistent with the measurements of cell cycle activity. In contrast, in heart sections from mice treated with AAV9-Cre at P8 and analyzed at 8 weeks of age, the proportion of tdTomato$^+$ cardiomyocytes was similar between control and *Tfam* mutant hearts (Online Figure XIIIB), consistent with *Tfam* inactivation at this stage having little effect on cardiomyocyte cell cycle activity.

These data collectively support a model in which mitochondrial dysfunction triggered by *Tfam* inactivation decreases neonatal cardiomyocyte proliferation through ROS-mediated DNA damage and activation of the G2/M cell cycle checkpoint. This impaired neonatal cardiomyocyte cell cycle activity contributes to adult ventricular dysfunction. Alleviating the inhibition of cardiomyocyte cell cycle activity, either by ROS scavenging or WEE1 kinase inhibition, improves cardiomyocyte cell cycle activity and thereby partially rescues heart function.

Mitochondria Are Dispensable for Postnatal Cardiomyocyte Maturation

During the neonatal period, cardiomyocytes undergo a dramatic phenotypic switch that includes tremendous physiological cardiomyocyte hypertrophy, increased sarcomere organization, and formation of T-tubules.[25,26] Concurrent with these structural changes is a switch from glycolytic to oxidative metabolism. In cardiomyocytes derived from stem cells, metabolic maturation influences cardiomyocyte differentiation,[27] and a similar role in neonatal cardiomyocyte maturation has been hypothesized.[28,29] Because *Tfam* is essential for normal cardiomyocyte metabolic maturation, we tested this hypothesis by assessing the postnatal maturation of *Tfam*-deficient cardiomyocytes. Previously, we showed that inactivation of genes in a fraction of cardiomyocytes is a powerful approach to study cell-autonomous function without impairing viability or eliciting nonspecific effects caused by cardiac dysfunction.[14,15] Low-dose AAV9-Cre ablated *Tfam* in transduced cardiomyocytes marked by tdTomato expression (Figure 6C; Online Figure XIIB) without measurably impairing cardiac function (Figure 6D and 6E). Therefore, we took advantage of this model to interrogate the effect of *Tfam* depletion on cardiomyocyte maturation.

Tfam$^{fl/+}$; Rosa26^{tdTomato} and Tfam$^{fl/fl}$; Rosa26^{tdTomato} mice were treated with low-dose AAV9-Cre at P0. We characterized the kinetics of mitochondrial dysfunction in these mice by measuring the expression of *mt-Atp6*, *mt-Nd1*, and *mt-Co1* genes encoded by the mitochondrial genome that require TFAM for transcription. After heart dissociation, tdTomato$^+$ cardiomyocytes were isolated by flow cytometry, and gene expression was measured by quantitative real-time PCR. By P14, all 3 transcripts were reduced by over 50%, and by P28 their expression was reduced by 85%, 80%, and 80%, respectively, compared with littermate Tfam$^{fl/+}$ controls (Online Figure XVA). These data suggest that mitochondrial dysfunction occurs rapidly in this model, within a window that would be anticipated to impact perinatal cardiomyocyte maturation.

We studied the cell-autonomous effect of mosaic *Tfam* ablation on cardiomyocyte maturation at 4 weeks of age. We used in situ confocal imaging, in which intact hearts are optically sectioned by confocal imaging, to examine T-tubule structure. Mitochondria and T-tubules were imaged by perfusion with mitoTracker and the voltage-sensitive membrane dye FM4-64 (*N*-(3-triethylammoniumpropyl)-4-(6-(4-(diethylamino) phenyl) hexatrienyl) pyridinium dibromide). These data showed that tdTomato$^+$ cells from Tfam$^{fl/fl}$ hearts had disrupted mitoTracker staining, consistent with effective *Tfam* depletion and mitochondrial disruption, yet had preserved T-tubule morphology (Figure 7A). We quantitatively analyzed T-tubule morphology of tdTomato$^+$ cells from low-dose AAV9-Cre–treated Tfam$^{fl/fl}$ and Tfam$^{fl/+}$ hearts using AutoTT software[16] (Figure 7B, 7D through 7G). There was no significant difference between genotypes. These data show that development of mature T-tubules, often considered a hallmark of cardiomyocyte maturation, does not require normal mitochondrial function.

To interrogate sarcomere structure, we dissociated cardiomyocytes by collagenase perfusion and immunostained them for sarcomeric α-actinin, which labels Z-lines (Figure 7C). Sarcomeric organization was also quantified using AutoTT. We found no significant difference in sarcomere regularity or spacing between AAV9-Cre–treated Tfam$^{fl/fl}$ and Tfam$^{fl/+}$ tdTomato$^+$ cardiomyocytes (Figure 7H and 7I). These results indicate that normal mitochondrial function is not required for attaining mature sarcomere organization.

Physiological hypertrophy of cardiomyocytes is another hallmark of cardiomyocyte maturation. We measured the length, length/width ratio, and area of dissociated, tdTomato$^+$ cardiomyocytes from Tfam$^{fl/fl}$ or Tfam$^{fl/+}$ hearts (Figure 7J through 7L). As with T-tubule and sarcomere organization, these parameters of cardiomyocyte hypertrophy were no different between genotypes, indicating that normal mitochondrial function is not required for physiological cardiomyocyte growth.

Switching of sarcomere isoforms is another hallmark of postnatal cardiomyocyte maturation.[26] We assessed the exchange of *Myh7* (immature) to *Myh6* (mature) and the switch of *Tnni1* (troponin I; immature) to *Tnni3* (mature). This latter isoform switch is specific to maturation and insensitive to cardiomyocyte stress.[30] We measured *Tnni3*, *Tnni1*, *Myh6*, and *Myh7* transcript levels by quantitative real-time PCR (Online Figure XVB). Expression of these genes, as well as the *Tnni3*/*Tnni1* and *Myh6*/*Myh7* ratio, was not significantly changed by *Tfam* inactivation, indicating that these gene expression markers of cardiomyocyte maturation were not perturbed by *Tfam* ablation.

Although *Tfam* inactivation had minimal effect on structural aspects of cardiomyocyte maturation, it did significantly impact 2 aspects of cardiomyocyte function: intracellular Ca^{2+} handling and contraction. To evaluate the effect of *Tfam* inactivation on intracellular Ca^{2+} handling, we treated Tfam$^{fl/fl}$; Rosa26^{tdTomato} and Tfam$^{fl/+}$; Rosa26^{tdTomato} mice with low-dose AAV9-Cre at P1, dissociated cardiomyocytes at P28, and loaded them with the Ca^{2+}-sensitive dye Fluo-4. Ca^{2+} transients were measured by confocal line scan during 1 Hz pacing (Figure 8A). *Tfam*-deficient cardiomyocytes exhibited significantly lower Ca^{2+} transient amplitude (F/F_0; Figure 8A and 8B). On the other hand, time to peak was not significantly different in *Tfam*-deficient cardiomyocytes (Figure 8A and 8C), consistent with the preserved T-tubule structure that we observed in these cells. *Tfam* inactivation also did not significantly affect

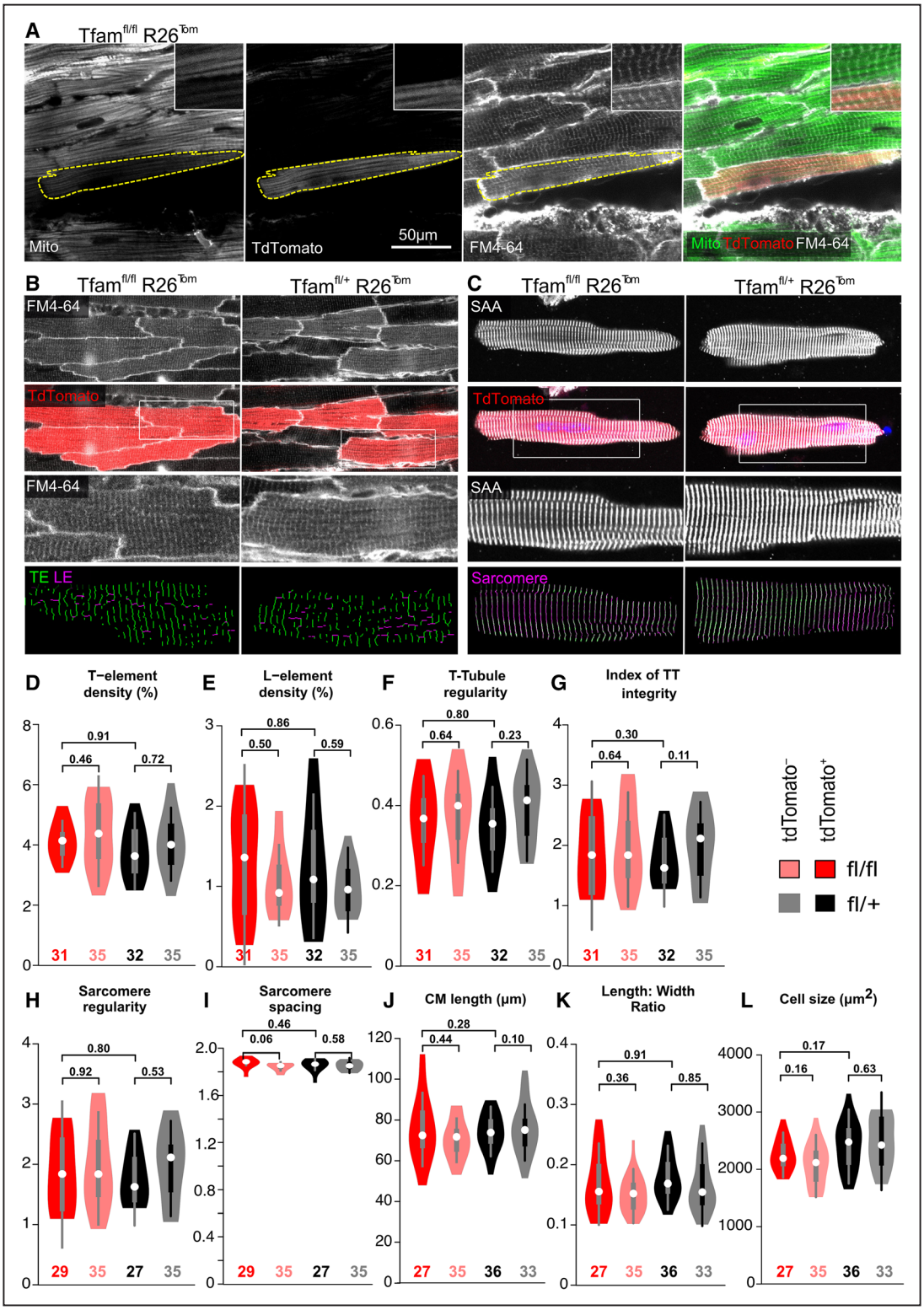

Figure 7. Mitochondria are dispensable for morphological postnatal cardiomyocyte (CM) maturation. A, In situ confocal live imaging of mitochondria and transverse tubules (T-tubules). Control and mosaic TFAM (mitochondrial transcription factor A)-depleted postnatal day 28 (P28) hearts were perfused with Mitotracker and FM4-64 (*N*-(3-triethylammoniumpropyl)-4-(6-(4-(diethylamino) phenyl) hexatrienyl) pyridinium dibromide) and optically sectioned. **B**, In situ confocal live imaging of T-tubules in FM4-64 loaded P28 hearts after control or mosaic TFAM depletion. The T-Tubule patterns in white boxes were enlarged and skeletonized using AutoTT. **C**, Imaging of sarcomeres in P28 CMs dissociated from hearts after control or mosaic TFAM depletion. Sarcomeres were visualized by sarcomeric α-actinin (SAA) staining. The boxed areas were enlarged (third row) and skeletonized (fourth row) using AutoTT. **D–G**, AutoTT quantification of T-tubule patterns visualized by in situ imaging. **H**, **I**, AutoTT quantification of sarcomere organization in isolated CMs. **J**, **K**, Quantification of CM dimensions. Length and width of SAA-stained dissociated CMs was determined using ImageJ. Violin plots show the distribution of values and the median (circle), 25th and 75th percentiles (thick line), and 1.5× the interquartile range (thin lines). Sample sizes are indicated by numbers above the abscissa. *P* values of intergroup comparisons using the Mann–Whitney *U* test are shown.

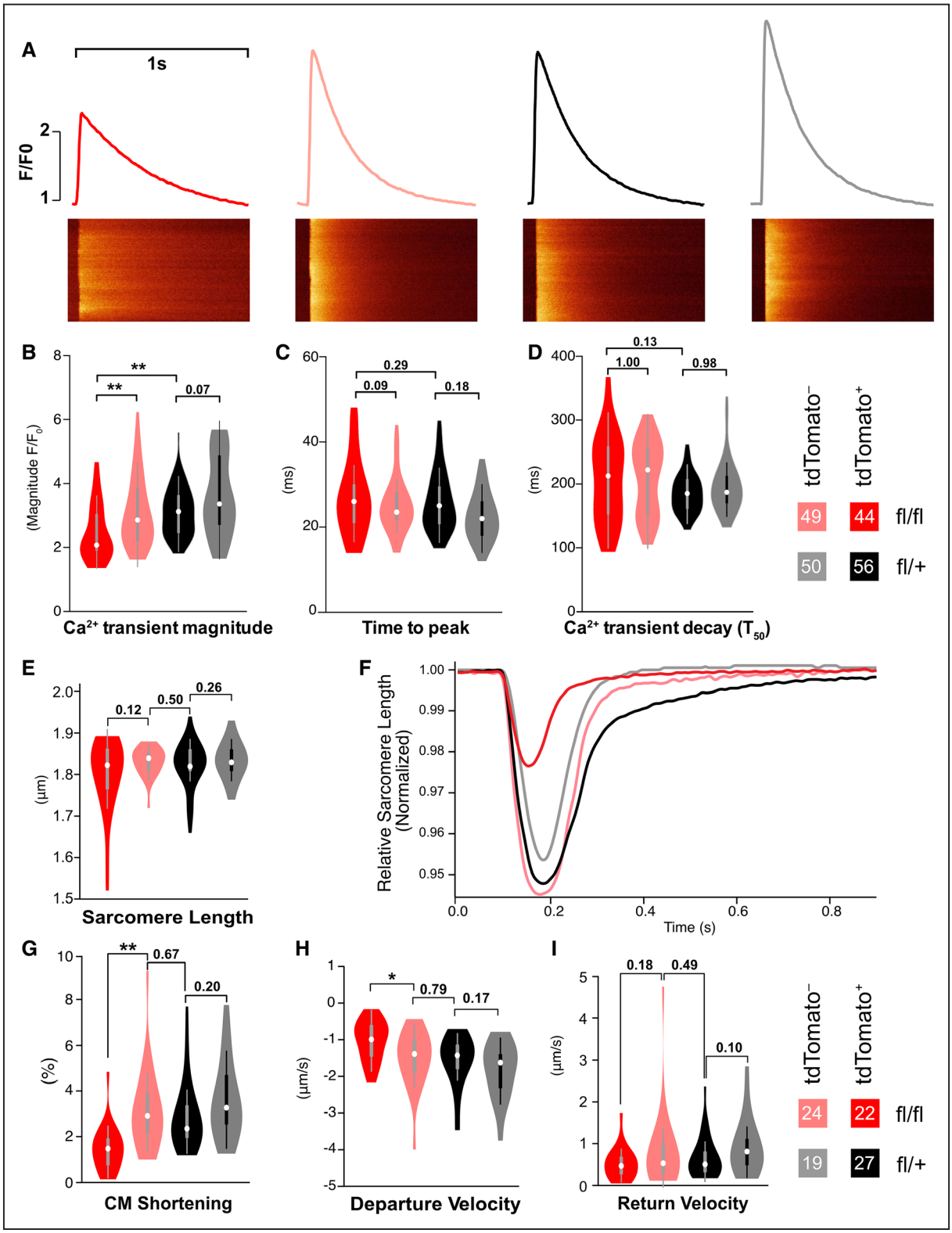

Figure 8. Cell-autonomous effect of *Tfam* (mitochondrial transcription factor A) inactivation on cardiomyocyte (CM) Ca^{2+} handling and contraction. A–D, Analysis of Ca^{2+} handling. Postnatal day 28 (P28) dissociated CMs were loaded with the Ca^{2+}-sensitive dye Fluo-4 AM and imaged by confocal line scan during 1 Hz pacing. **A**, Representative Ca^{2+} transient profiles are shown. Ca^{2+} transient magnitude, time to peak, and time to 50% recovery were quantitative analyzed (**B–D**). **E–I**, Analysis of contraction. Bright-field images of dissociated P28 CMs contracting during 1 Hz pacing were recorded. Image analysis yielded sarcomere length of live cells (**E**) and length–time relationship during contraction (**F**). Analysis of the length–time relationship yielded the fractional CM shortening (**G**), departure velocity (**H**), and return velocity (**I**). Violin plots show the distribution of values and the median (circle), 25th and 75th percentiles (thick line), and 1.5× the interquartile range (thin lines). Numbers within graph legend indicate the number of CMs analyzed. These CMs were isolated from 4 hearts per group. Groups were compared by Mann–Whitney *U* test. **P*<0.05. ***P*<0.01. ****P*<0.001.

time to 50% decay (Figure 8A and 8D), a measure of the kinetics of cytosolic Ca^{2+} return to diastolic levels.

To assess the effect of *Tfam* inactivation on cardiomyocyte contraction, we prepared dissociated $Tfam^{fl/fl}$; $Rosa26^{tdTomato}$ and $Tfam^{fl/+}$; $Rosa26^{tdTomato}$ cardiomyocytes as described for the Ca^{2+} handling experiments. Bright-field images of the cardiomyocytes were obtained during 1 Hz pacing. Consistent with immunostaining of fixed cells, sarcomere length from these live cells was not different between *Tfam*-deficient and control cardiomyocytes (Figure 8E). However, *Tfam*-deleted cardiomyocytes had significantly reduced shortening and departure velocity compared with the other groups (Figure 8F through 8H), consistent with reduced contractility and lower Ca^{2+} transient amplitude. *Tfam*-deficient cardiomyocytes did not have significantly altered return velocity, suggesting that cardiomyocyte relaxation was not significantly affected (Figure 8I). These data indicate that *Tfam*-deficient cardiomyocytes have reduced contractility compared with control cardiomyocytes.

Collectively, these data support the surprising conclusion that morphological cardiomyocyte maturation is not dependent on their metabolic maturation. However, *Tfam* is required for normal cardiomyocyte Ca^{2+} handling and contraction.

Discussion

Although cardiomyopathy and abnormal myocardial morphologies such as left ventricular noncompaction and hypertrophic cardiomyopathy are associated with mitochondrial disease, the mechanisms linking mitochondria to these morphological findings have been understudied. Although energy depletion likely contributes to these phenotypes, our study highlights the effect that mitochondrial dysfunction has on another basic process of cardiac development, namely cardiomyocyte proliferation. We observed that mitochondrial dysfunction triggered by *Tfam* ablation induces cell cycle arrest that contributes to the resulting mitochondrial cardiomyopathy. Protecting cardiomyocytes from cell cycle arrest induced by mitochondrial dysfunction improved cardiac function for weeks beyond the treatment period, suggesting a potential therapeutic strategy for mitochondrial cardiomyopathies.

Although *Tfam* inactivation reduced mitochondrial mass, we observed that it increased mitochondrial ROS in cardiomyocytes. The effect of *Tfam* inactivation on mitochondrial ROS seems to be cell type dependent because it was previously observed to elevate ROS in adipocytes[8] and reduce ROS in keratinocytes.[19] The cell types in which it elevated ROS (cardiomyocytes and adipocytes) are normally rich in mitochondria, suggesting a potential factor responsible for the difference between cell types. A potential mechanism that accounts for elevated ROS in *Tfam*-deficient cardiomyocytes is the markedly reduced expression of components of the electron transport chain encoded by the mitochondrial genome.[8] The defective electron transport chain of *Tfam*-deficient cardiomyocytes may be predisposed to produce ROS. In normal mitochondria, membrane depolarization accelerates electron transit through the electron transport chain and thereby reduces ROS production[31]; however, increased activity of the defective electron transport chain of *Tfam*-deficient cardiomyocytes may elevate ROS production.

Elevated ROS in *Tfam*-depleted cardiomyocytes induced the DNA damage response, including deposition of γH2A.X. As a result, inhibitory cell cycle checkpoints were activated, resulting in reduced cardiomyocyte cell cycle activity. Elevated cardiomyocyte ROS triggered by increased mitochondrial oxidative phosphorylation in the oxygen-rich postnatal environment has been proposed to trigger physiological cell cycle arrest of neonatal cardiomyocytes through a similar mechanism.[17] That WEE1 kinase inhibition alleviated cell cycle exit induced by *Tfam* inactivation suggests that the main checkpoint occurred at the G2/M transition, where cell cycle progression requires CDC25 dephosphorylation of CKD1 to overcome its phosphorylation by WEE1 kinase.[22]

Our data suggest that inhibition of cardiomyocyte cell cycle activity may be an important contributor to some forms of mitochondrial cardiomyopathy. In our model, mitochondrial dysfunction was triggered in neonatal mice by delivery of AAV9-Cre at P0 or P1. Remarkably, transient treatment of neonatal mice during the first postnatal week with either ROS scavenger or WEE1 inhibitor ameliorated heart dysfunction as much as 7 weeks later. That this same treatment did not have benefit when given in the second postnatal week suggests that these treatments primarily work by maintaining cardiomyocyte cell cycle activity because the therapeutic window coincides with the period during which neonatal cardiomyocytes normally retain cell cycle activity. A corollary to this interpretation is that increased abundance of *Tfam*-deficient cardiomyocytes supports increased cardiac contraction. Indeed, we observed that *Tfam*-deficient cardiomyocytes do contract, albeit more weakly than littermate control cardiomyocytes. The important contribution of reduced cardiomyocyte proliferation to the *Tfam* mutant cardiomyopathic phenotype was further corroborated by the observation that *Tfam* inactivation at P8 (after cardiomyocyte cell cycle exit) was less deleterious to heart function than its inactivation at P1 (during cardiomyocyte proliferation). In future work, it will be important to determine the durability of the improvement in heart function induced by MT or MK treatment. It is interesting to consider that some human cardiomyopathies, such as those caused by a subset of mitochondrial diseases, might exhibit a similar window during which myocardial outcome could be improved by neonatal therapy. Further research will be needed to evaluate the relevance of our observations in the Tfam-knockout model to human mitochondrial cardiomyopathy.

Neonatal cardiomyocytes undergo many phenotypic changes that convert them from proliferative fetal cells with relatively low pumping capability to mature, terminally differentiated, adult cardiomyocytes with much higher pumping capacity.[25,26] Accompanying these changes is a metabolic switch from glycolysis to oxidative phosphorylation, and this metabolic switch has been hypothesized to help to drive the other phenotypic changes.[27–29] Using postnatal mosaic *Tfam* inactivation, we critically tested this hypothesis. Surprisingly, we found that cardiomyocyte growth, sarcomeric organization, and T-tubule formation were unaffected by neonatal *Tfam* inactivation. These data suggest that mitochondrial expansion and robust function are not prerequisites for morphological cardiomyocyte maturation in vivo, although they are required for normal Ca^{2+} handling and contraction. However, this result does

not exclude the possibility that enhancing metabolic maturation of iPSC (induced pluripotent stem cells) cardiomyocytes will expedite their morphological and functional maturation.

Sources of Funding

W.T. Pu was funded by the Barth Syndrome Foundation and R01 HL128694. Y. Li was funded by Technology Project of Sichuan Province of China 2016SZ0056. S. Guatimosim was a recipient of a Coordenação de Aperfeiçoamento de Pessoal de Nível Superior fellowship and funded by Conselho Nacional de Desenvolvimento Científico e Tecnológico and Fundação de Amparo a Pesquisa do Estado de Minas Gerais.

Disclosures

None.

References

1. Koopman WJ, Willems PH, Smeitink JA. Monogenic mitochondrial disorders. *N Engl J Med*. 2012;366:1132–1141. doi: 10.1056/NEJMra1012478.
2. Wang G, McCain ML, Yang L, et al. Modeling the mitochondrial cardiomyopathy of Barth syndrome with induced pluripotent stem cell and heart-on-chip technologies. *Nat Med*. 2014;20:616–623. doi: 10.1038/nm.3545.
3. Hom JR, Quintanilla RA, Hoffman DL, de Mesy Bentley KL, Molkentin JD, Sheu SS, Porter GA Jr. The permeability transition pore controls cardiac mitochondrial maturation and myocyte differentiation. *Dev Cell*. 2011;21:469–478. doi: 10.1016/j.devcel.2011.08.008.
4. Lai L, Leone TC, Zechner C, Schaeffer PJ, Kelly SM, Flanagan DP, Medeiros DM, Kovacs A, Kelly DP. Transcriptional coactivators PGC-1alpha and PGC-lbeta control overlapping programs required for perinatal maturation of the heart. *Genes Dev*. 2008;22:1948–1961. doi: 10.1101/gad.1661708.
5. Karamanlidis G, Lee CF, Garcia-Menendez L, Kolwicz SC Jr, Suthammarak W, Gong G, Sedensky MM, Morgan PG, Wang W, Tian R. Mitochondrial complex I deficiency increases protein acetylation and accelerates heart failure. *Cell Metab*. 2013;18:239–250. doi: 10.1016/j.cmet.2013.07.002.
6. Ke BX, Pepe S, Grubb DR, Komen JC, Laskowski A, Rodda FA, Hardman BM, Pitt JJ, Ryan MT, Lazarou M, Koleff J, Cheung MM, Smolich JJ, Thorburn DR. Tissue-specific splicing of an Ndufs6 gene-trap insertion generates a mitochondrial complex I deficiency-specific cardiomyopathy. *Proc Natl Acad Sci USA*. 2012;109:6165–6170. doi: 10.1073/pnas.1113987109.
7. Kang D, Kim SH, Hamasaki N. Mitochondrial transcription factor A (TFAM): roles in maintenance of mtDNA and cellular functions. *Mitochondrion*. 2007;7:39–44. doi: 10.1016/j.mito.2006.11.017.
8. Vernochet C, Mourier A, Bezy O, et al. Adipose-specific deletion of TFAM increases mitochondrial oxidation and protects mice against obesity and insulin resistance. *Cell Metab*. 2012;16:765–776. doi: 10.1016/j.cmet.2012.10.016.
9. Li H, Wang J, Wilhelmsson H, Hansson A, Thoren P, Duffy J, Rustin P, Larsson NG. Genetic modification of survival in tissue-specific knockout mice with mitochondrial cardiomyopathy. *Proc Natl Acad Sci USA*. 2000;97:3467–3472.
10. Wang J, Wilhelmsson H, Graff C, Li H, Oldfors A, Rustin P, Brüning JC, Kahn CR, Clayton DA, Barsh GS, Thorén P, Larsson NG. Dilated cardiomyopathy and atrioventricular conduction blocks induced by heart-specific inactivation of mitochondrial DNA gene expression. *Nat Genet*. 1999;21:133–137. doi: 10.1038/5089.
11. Stanley EG, Biben C, Elefanty A, Barnett L, Koentgen F, Robb L, Harvey RP. Efficient Cre-mediated deletion in cardiac progenitor cells conferred by a 3'UTR-ires-Cre allele of the homeobox gene Nkx2-5. *Int J Dev Biol*. 2002;46:431–439.
12. Ventura A, Kirsch DG, McLaughlin ME, Tuveson DA, Grimm J, Lintault L, Newman J, Reczek EE, Weissleder R, Jacks T. Restoration of p53 function leads to tumour regression in vivo. *Nature*. 2007;445:661–665. doi: 10.1038/nature05541.
13. Madisen L, Zwingman TA, Sunkin SM, Oh SW, Zariwala HA, Gu H, Ng LL, Palmiter RD, Hawrylycz MJ, Jones AR, Lein ES, Zeng H. A robust and high-throughput Cre reporting and characterization system for the whole mouse brain. *Nat Neurosci*. 2010;13:133–140. doi: 10.1038/nn.2467.
14. Prendiville TW, Guo H, Lin Z, Zhou P, Stevens SM, He A, VanDusen N, Chen J, Zhong L, Wang DZ, Gao G, Pu WT. Novel roles of GATA4/6 in the postnatal heart identified through temporally controlled, cardiomyocyte-specific gene inactivation by adeno-associated virus delivery of Cre recombinase. *PLoS One*. 2015;10:e0128105. doi: 10.1371/journal.pone.0128105.
15. Guo Y, VanDusen NJ, Zhang L, Gu W, Sethi I, Guatimosim S, Ma Q, et al. Analysis of cardiac myocyte maturation using CASAAV, a platform for rapid dissection of cardiac myocyte gene function in vivo. *Circ Res*. 2017;120:1874–1888. doi: 10.1161/CIRCRESAHA.116.310283.
16. Guo A, Song LS. AutoTT: automated detection and analysis of T-tubule architecture in cardiomyocytes. *Biophys J*. 2014;106:2729–2736. doi: 10.1016/j.bpj.2014.05.013.
17. Puente BN, Kimura W, Muralidhar SA, et al. The oxygen-rich postnatal environment induces cardiomyocyte cell-cycle arrest through DNA damage response. *Cell*. 2014;157:565–579. doi: 10.1016/j.cell.2014.03.032.
18. Subramanian A, Tamayo P, Mootha VK, Mukherjee S, Ebert BL, Gillette MA, Paulovich A, Pomeroy SL, Golub TR, Lander ES, Mesirov JP. Gene set enrichment analysis: a knowledge-based approach for interpreting genome-wide expression profiles. *Proc Natl Acad Sci USA*. 2005;102:15545–15550. doi: 10.1073/pnas.0506580102.
19. Hamanaka RB, Glasauer A, Hoover P, Yang S, Blatt H, Mullen AR, Getsios S, Gottardi CJ, DeBerardinis RJ, Lavker RM, Chandel NS. Mitochondrial reactive oxygen species promote epidermal differentiation and hair follicle development. *Sci Signal*. 2013;6:ra8. doi: 10.1126/scisignal.2003638.
20. Singh RK, Saini S, Verma D, Kalaiarasan P, Bamezai RNK. Mitochondrial ND5 mutation mediated elevated ROS regulates apoptotic pathway epigenetically in a P53 dependent manner for generating pro-cancerous phenotypes. *Mitochondrion*. 2017;35:35–43. doi: 10.1016/j.mito.2017.05.001.
21. Revet I, Feeney L, Bruguera S, Wilson W, Dong TK, Oh DH, Dankort D, et al. Functional relevance of the histone γH2Ax in the response to DNA damaging agents. *Proc Natl Acad Sci USA*. 2011;108:8663–8667.
22. Rhind N, Russell P. Signaling pathways that regulate cell division. *Cold Spring Harb Perspect Biol*. 2012;4:a005942. doi: 10.1101/cshperspect.a005942.
23. Porrello ER, Mahmoud AI, Simpson E, Hill JA, Richardson JA, Olson EN, Sadek HA. Transient regenerative potential of the neonatal mouse heart. *Science*. 2011;331:1078–1080. doi: 10.1126/science.1200708.
24. Soonpaa MH, Kim KK, Pajak L, Franklin M, Field LJ. Cardiomyocyte DNA synthesis and binucleation during murine development. *Am J Physiol*. 1996;271:H2183–H2189.
25. Yang X, Pabon L, Murry CE. Engineering adolescence: maturation of human pluripotent stem cell-derived cardiomyocytes. *Circ Res*. 2014;114:511–523. doi: 10.1161/CIRCRESAHA.114.300558.
26. Galdos FX, Guo Y, Paige SL, VanDusen NJ, Wu SM, Pu WT. Cardiac regeneration: lessons from development. *Circ Res*. 2017;120:941–959. doi: 10.1161/CIRCRESAHA.116.309040.
27. Chung S, Dzeja PP, Faustino RS, Perez-Terzic C, Behfar A, Terzic A. Mitochondrial oxidative metabolism is required for the cardiac differentiation of stem cells. *Nat Clin Pract Cardiovasc Med*. 2007;4(suppl 1):S60–S67. doi: 10.1038/ncpcardio0766.
28. Lopaschuk GD, Jaswal JS. Energy metabolic phenotype of the cardiomyocyte during development, differentiation, and postnatal maturation. *J Cardiovasc Pharmacol*. 2010;56:130–140. doi: 10.1097/FJC.0b013e3181e74a14.
29. Ellen Kreipke R, Wang Y, Miklas JW, Mathieu J, Ruohola-Baker H. Metabolic remodeling in early development and cardiomyocyte maturation. *Semin Cell Dev Biol*. 2016;52:84–92. doi: 10.1016/j.semcdb.2016.02.004.
30. Bedada FB, Chan SS, Metzger SK, Zhang L, Zhang J, Garry DJ, Kamp TJ, Kyba M, Metzger JM. Acquisition of a quantitative, stoichiometrically conserved ratiometric marker of maturation status in stem cell-derived cardiac myocytes. *Stem Cell Reports*. 2014;3:594–605. doi: 10.1016/j.stemcr.2014.07.012.
31. Brand MD. Mitochondrial generation of superoxide and hydrogen peroxide as the source of mitochondrial redox signaling. *Free Radic Biol Med*. 2016;100:14–31. doi: 10.1016/j.freeradbiomed.2016.04.001.